RSC Advances

ROYAL SOCIETY OF CHEMISTRY

www.rsc.org/advances

Conversion of CO_2 into Renewable Fuel over Pt-g-C_3N_4/$KNbO_3$ composite photocatalyst

Haifeng Shi, [a, b] Chengliang Zhang, [a,b] Changping Zhou, [a,b] and Guoqing Chen, [a,b]

[a] School of science, Jiangnan University, Wuxi, 214122, P. R. China

[b] Jiangsu Provincial Research Center of Light Industrial Optoelectronic Engineering and Technology, Jiangnan University, Wuxi, 214122, P. R. China

Dr. Haifeng Shi

School of Science, Jiangnan University

Wuxi, P. R. China, 214122

E-mail: hfshi@jiangnan.edu.cn (HF Shi)

Conversion of CO_2 into Renewable Fuel over Pt-g-C_3N_4/$KNbO_3$ composite photocatalyst

Haifeng Shi, [a, b] Chengliang Zhang, [a,b] Changping Zhou, [a,b] and Guoqing Chen, [a,b]

[a] School of science, Jiangnan University, Wuxi, 214122, P. R. China

[b] Jiangsu Provincial Research Center of Light Industrial Optoelectronic Engineering and Technology, Jiangnan University, Wuxi, 214122, P. R. China

Abstract: g-C_3N_4/$KNbO_3$ composites were fabricated by ultrasonic dispersion followed by heat treatment method, and developed as visible-light-sensitive photocatalysts for CO_2 conversion. The photocatalysts were characterized by X-ray powder diffraction, scanning electron microscopy, transmission electron microscopy, X-ray photoelectron spectroscopy, photoluminescence spectra, nitrogen adsorption-desorption, and UV–Vis diffuse reflection spectroscopy. The HRTEM revealed that an intimate interface between g-C_3N_4 and $KNbO_3$ was formed in g-C_3N_4/$KNbO_3$ composite. The g-C_3N_4/$KNbO_3$ composite exhibited the superior photocatalytic performance for CO_2 reduction compared to g-C_3N_4 under visible-light illumination. Such a significant enhancement in the photocatalytic activity was mainly ascribed to the improved separation efficiency of photoinduced carriers in the interface of g-C_3N_4/$KNbO_3$ composite, which was beneficial for separating the photoinduced electron-holes and thus improving the photocatalytic performance. The present study would provide a useful method to develop an effective composite

photocatalyst for CO_2 reduction under visible light irradiation.

Keywords: Potassium niobate, composite photocatalyst, g-C_3N_4, carbon dioxide, conversion.

1. Introduction

The increasing anthropogenic carbon dioxide (CO_2) emission is widely recognized as one of the primary causes of the greenhouse effect, resulting in climate problems such as severe weather events increase and sea levels raise. The development of an artificial photosynthetic system is undoubtedly a promising strategy to photocatalytic conversion of CO_2 into useful solar fuels, excepting the carbon capture and sequestration technology. [1] Although the conversion of CO_2 is a quite intensive challenging task due to its relatively inertness with a closed-shell electronic configuration and good stability, but the photocatalytic reduction of CO_2 into fuels utilizing photocatalysts and sunlight appears to be a favorable technology to solve this challenge owing to the potential ability to produce renewable energy as well as alleviate the greenhouse effect.[2-9] Research in this field was initially triggered by the demonstration of photocatalytic reduction of CO_2 into hydrocarbon products (such as formaldehyde, methanol, formic acid, and methane) over TiO_2 particles in 1979.[10] After this pioneering breakthrough, extensive attempts have been directed to exploit the efficient photocatalytic systems for CO_2 reduction that occur on the solid-liquid interface or the solid-gas interfaces in the semiconductor photocatalysts.[10-15] Among the various semiconductor photocatalysts, TiO_2 with the obvious benefits of chemical stability and nontoxicity has been extensively investigated as a classic photocatalyst, which is only active under the ultraviolet (UV) light irradiation owing to the relative

wide band gap. [16,17] Actually, in addition to TiO_2, several UV or visible-light responsive photocatalysts, such as metal oxide, metal sulfides, and homogeneous organometallic materials, have been developed for CO_2 reduction over the past more than three decades.[18-27] However, the solar-to-chemical energy conversion efficiencies of the reported photocatalysts are still not high enough for making these systems commercially practicable up to date.

Recently, a metal-free π-conjugated photocatalyst, graphitic carbon nitride (g-C_3N_4) with high chemical stability and nontoxicity, is receiving considerable attention owing to its potential applications, such as water splitting, organic pollutant degradation, and CO_2 reduction.[28-35] Since Wang and co-workers firstly reported g-C_3N_4 as a novel photocatalyst for hydrogen production from water under visible light illumination,[36] many efforts have been made to improve its photocatalytic performance. Unfortunately, the photocatalytic efficiency of g-C_3N_4 is still far from optimum due to the inevitable high recombination rate of photogenerated electron-hole, which is generally regarded as a major obstacle in the single-component semiconductor photocatalyst. Among the various means to enhance the photocatalytic activity, constructing heterostructured composites by coupling two proper photocatalysts is generally recognized as one of the effective methods. In a composite photocatalyst, the separation efficiency of the photogenerated charge would increase and thus improve the photocatalytic activity if the two pristine photocatalysts possess the properly relative positions of conduction band (CB) and valence band (VB). In view of the advantages of manufacturing composites photocatalysts, several kinds of g-C_3N_4-based composite photocatalysts have been successfully exploited and showed evidently superior photocatalytic performance than those of the pristine materials comprising the composites, which mainly focused on

organic decomposition and/or hydrogen evolution.[37-50] However, to the best of our knowledge, the reports about the C_3N_4 composite photocatalysts for photocatalytic CO_2 reduction are still limited,[51-55] thus we envision developing some new g-C_3N_4-based composite photocatalysts as the potential candidates to test the photocatalytic CO_2 reduction performance.

Environmentally benign potassium niobate ($KNbO_3$) with a typical ABO_3 pervoskite-structure is attracting much interest in both scientific and engineering areas due to its various interesting properties, such as ferroelectric, piezoelectric, and ionic conductive. Recently, $KNbO_3$ was reported as an efficient photocatalyst for water splitting and CO_2 reduction.[56-61] Herein, in this study, g-C_3N_4 and $KNbO_3$ were employed as two candidates for constructing g-C_3N_4/$KNbO_3$ composite photocatalysts. The physical properties of samples were examined by the following characterizations, such as X-ray diffraction, UV-visible diffuse reflectance spectroscopy, X-ray photoelectron spectroscopy, nitrogen adsorption-desorption, scanning electron microscopy, photoluminescence spectra, and high-resolution transmission electron microscopy, respectively. Interestingly, we found that the as-prepared g-C_3N_4/$KNbO_3$ composite photocatalyst exhibited an enhanced photocatalytic CH_4 production in visible-light-driven CO_2 reduction. A possible mechanism for the improved photocatalytic performance of g-C_3N_4/$KNbO_3$ was tentatively proposed based on the process of photoinduced carries transfer and separation.

2. Experimental Section

2.1 Catalyst synthesis

All chemical reagents were analytical pure and used as received without further purification. $KNbO_3$ were synthesized through a hydrothermal treatment method. In a

typical case, 0.3 g Nb_2O_5 and 14 g KOH were dissolved in 25 mL deionized H_2O. Subsequently, the mixture was constantly stirred for 4 h and then poured into a Teflon-lined autoclave with a heat treatment at 150 °C for 3 days. After cooling to room temperature, the obtained precipitate was washed thoroughly with distilled water several times and dried in an oven at 80 °C for 12 h. The metal-free g-C_3N_4 powders were synthesized by heating melamine in air at 520 °C for 4 h in a muffle furnace. The resulting yellow products were naturally cooled to room temperature and ground into powders. The g-C_3N_4/$KNbO_3$ composites were prepared as follows: firstly, the methanol solution containing g-C_3N_4 and $KNbO_3$ (25 wt % $KNbO_3$) was ultrasonicated for 60 min and then constantly stirred for 6 h. After that, the product was washed with distilled water and dried in an oven at 90 °C for 24 h. Finally, the obtained samples were heated to 500 °C for 2 h. For comparison, the g-C_3N_4 powder was also treated with the same treatment process of composite. The Pt loaded photocatalysts were synthesized by an in situ photodeposition method. Typically, 0.1 g photocatalyst, 40 mL distilled water, 25 mL CH_3OH and a given amount of $H_2PtCl_6 \cdot 6H_2O$ (0.5 wt %) were placed in a glass vessel. The reactant solution was irradiated by a 300 W Xe arc lamp for 8 h with constantly stirring. Then the Pt-loaded photocatalysts were filtered and washed thoroughly with deionized water, subsequently dried at 80 °C for 24 h.

2.2 Catalysis characterization

The compositions and crystal structures of samples were identified by a powder X-ray diffractometer (DX2700, Dandong, China) employing Cu Kα radiation in the

2θ range of 10-90º. The diffuse reflectance spectra of the samples were measured using a UV-vis spectrophotometer (UV-2600; Shimadzu, Japan) equipped with an integrating sphere attachment. Morphologies of samples were characterized by a field-emission scanning electron microscope (FE-SEM; FEI Tecnai G2 F30, USA) equipped with an energy-dispersive X-ray spectroscopy (EDS) and a high resolution transmission electron microscope (HRTEM; FEI Tecnai G20, USA). X-ray photoelectron spectroscopy (XPS) analysis was carried on a multifunctional imaging electron spectrometer (Thermo ESCALAB 250XI, USA) using an Al Kα monochromatic X-ray radiation. The surface areas were determined by the Brunauer-Emmett-Teller (BET) method with a surface area and porosimetry analyzer (Quadrasorb evo, USA). The XPS spectra were calibrated by the C–C bonds at 284.6 eV. Photoluminescence (PL) spectra were characterized at room temperature using a fluorescence spectrophotometer (FLS 920P, Edinburgh, England) with an excitation wavelength in 350 nm.

2.3 Photocatalytic activity evolution

In the photocatalytic reduction of CO_2, the photocatalyst (100 mg) was uniformly and evenly spread on the bottom of a small glass cell that was placed in the bottom of a Pyrex glass cell, which was attached with a gaseous closed system. A 300 W xenon arc lamp was employed as the light source for the photocatalytic reaction. After the reaction apparatus was vacuum-treated several times, the high purity of CO_2 gas and 2 mL of H_2O were injected into the reaction apparatus to realize ambient pressure. In order to obtain an adsorption-desorption equilibrium, the reactor was stored in the

dark condition for 2 h with a gas pump to accelerate gas diffusion. Subsequently, the reactor was irradiated from a 300-W Xe lamp quipped with a UV cutoff filter ($\lambda > 420$ nm). During the irradiation, a given gaseous sample was continually taken from the reaction cell at a given interval to examine the concentration of CH_4 using a gas chromatograph (GC-9790A, Fuli, China).

3. Results and Discussion

3.1. Characterization of g-C_3N_4/$KNbO_3$ composites.

The powder XRD patterns of g-C_3N_4/$KNbO_3$ composite, as well as those of g-C_3N_4 and $KNbO_3$ are presented in Fig. 1. No impurity phase was observed in $KNbO_3$, which was in good agreement with the XRD patterns of orthorhombic structured $KNbO_3$ in the JCPDS card (no. 32-0822). The two distinct peaks recorded in g-C_3N_4 XRD patterns were founded at 27.4º and 13.1º, which could be indexed as the (002) and (100) diffraction planes (JCPDS card: no. 87-1526), corresponding to the characteristic interplanar staking peaks of aromatic systems and the inter-layer structural packing,[62] respectively. The XRD patterns of g-C_3N_4/$KNbO_3$ revealed the coexistence peaks of both $KNbO_3$ and g-C_3N_4, indicating the presence of two phases in the composite. Furthermore, the BET surface area of g-C_3N_4, g-C_3N_4/$KNbO_3$, and $KNbO_3$ were measured to be 10.1, 9.4, and 12.0 $m^2 g^{-1}$, respectively.

Fig. 2 displays the UV-vis absorption spectra of $KNbO_3$, g-C_3N_4, and g-C_3N_4/$KNbO_3$, which are transformed from the diffuse reflection spectra according to the Kubelka-Munk relation. The absorbance edge of white colored $KNbO_3$ was located at approximately 365 nm, whereas the yellow colored g-C_3N_4 sample could absorb visible light up to 460 nm. The g-C_3N_4/$KNbO_3$ composite exhibited a similar

adsorption shoulder and a slight red shift tail on the adsorption edge that reached further out in the visible region, which was similar to the previous report.[63] This clearly demonstrated that g-C_3N_4/$KNbO_3$ had potential applications in the visible-light region. The optical band gap E_g of a semiconductor could be deduced according to the following equation: $(\alpha h\nu)^n = A(h\nu - E_g)$, where α, $h\nu$, A, E_g, n mean the absorption coefficient, the incident photo energy, a proportionality constant related to the material, the band gap energy of the semiconductor, and $n_{direct} = 2$ (or $n_{indirect} = 1/2$), respectively. As shown in the inset of Fig. 2b, the band gap energies were obtained from the intercept of the tangent line in the plot of $(\alpha h\nu)^{1/2}$ *vs* energy, and the values of g-C_3N_4 and $KNbO_3$ were determined to be 2.7 eV and 3.2 eV, respectively, which were in consistent with the values in the previous reports. [29,63]

The surface chemical compositions and states of the g-C_3N_4, $KNbO_3$, and g-C_3N_4/$KNbO_3$ were further investigated by X-ray photoelectron spectroscopy in order to investigate the interaction between $KNbO_3$ and g-C_3N_4. Fig. 3 shows C 1s and N 1s peaks of g-C_3N_4 and g-C_3N_4/$KNbO_3$, as well as K 2p, Nb 3d, and O 1s peaks for $KNbO_3$ and g-C_3N_4/$KNbO_3$, which are undoubtedly in agreement with the chemical composition in the photocatalysts. All the binding energies were referenced to the C 1s peak at 284.6 eV of the surface adventitious carbon. As displayed in the XPS spectra of C 1s (Fig. 3a), the strong peak (288.1 eV) in g-C_3N_4 could be assigned to sp^2-bonded carbon in N-containing aromatic rings (N–C=N); [64,65] while g-C_3N_4/$KNbO_3$ displayed a slightly lower binding energy of C 1s (287.9 eV) than that of pure g-C_3N_4. The inner shift of the C 1s peak possibly originated from the hybridization effect between g-C_3N_4 and $KNbO_3$. As displayed in Fig. 3b, N 1s peak located at 398.9 eV (g-C_3N_4) and 398.8 eV (g-C_3N_4/$KNbO_3$) originated from C=N-C coordination.[66] The binding energies of K $2p_{3/2}$ (290.7 eV) and K $2p_{1/2}$ (293.4 eV) for

$KNbO_3$ were much lower than those of K $2p_{3/2}$ (292.5 eV) and K $2p_{1/2}$ (295.2 eV) in g-C_3N_4/ $KNbO_3$ (see in Fig. 3c). In addition, the binding energies of Nb $3d_{3/2}$ (208.7 eV), Nb $3d_{5/2}$ (206.0 eV) and O 1s (528.9 eV) of pure $KNbO_3$ were slightly lower than those of Nb $3d_{3/2}$ (209.3 eV), Nb $3d_{5/2}$ (206.6 eV) and O 1s (529.6 eV) of g-C_3N_4/$KNbO_3$ (see in Fig. 3d,e).This implied that chemical interaction was possibly exited between $KNbO_3$ and g-C_3N_4.[63] In addition, the content was estimated by XPS measurement. The molar ratio of C_3N_4 and $KNbO_3$ is ~ 5.4 :1, corresponding to the mass ratio of g-C_3N_4 and $KNbO_3$ (2.8:1).

The morphologies and microstructures of g-C_3N_4, $KNbO_3$, and g-C_3N_4/$KNbO_3$ samples were checked by FE-SEM. Fig. 4 displays the FE-SEM images of g-C_3N_4, $KNbO_3$, and g-C_3N_4/$KNbO_3$ composite. It was revealed that g-C_3N_4 showeds the aggregated layered structure with several stacking layers (Fig. 4a). As shown in Fig. 4b, the $KNbO_3$ sample displayed as the stacked structures, which consisted of cube-shaped particles with several hundred nanometers in size. As displayed in Fig. 4c, amounts of $KNbO_3$ were found to randomly deposit and distribute on the surface of g-C_3N_4, resulting in forming a heterostructured g-C_3N_4/$KNbO_3$ material. Further EDX results (Fig. S1) indicated that the composite sample was composed of C, N, K, Nb, and O elements. Additionally, the EDS element maps of the composite displayed the element distribution of g-C_3N_4/$KNbO_3$, which was consistent with that in the SEM images. Aiming at getting the further information about the microstructures of the g-C_3N_4/$KNbO_3$, HRTEM analysis was performed. Fig. 5 shows the low- and high-magnification TEM images of the as-prepared g-C_3N_4/$KNbO_3$. Based on the observed morphologies of $KNbO_3$ and g-C_3N_4 in SEM images (Fig. 4), the dark parts in the TEM image (Fig. 5a) should correspond to $KNbO_3$ while the light parts were ascribed to C_3N_4, which further implies that $KNbO_3$ are located on the surface of

g-C_3N_4. It was note that the ultrasonication in TEM measurement do not peel off the composite due to the strong interaction between g-C_3N_4 and $KNbO_3$. Additionally, smooth and clear interfaces were observed between the g-C_3N_4 and $KNbO_3$, which implied the formation of g-C_3N_4/$KNbO_3$ composites. As shown in Fig. 5b, the clear lattice fringe in HRTEM should be ascribed to $KNbO_3$, and the d spacing value was 0.286 nm, corresponding to the (110) plane of orthorhombic-structured $KNbO_3$; While the low crystallinity with blurry lattices corresponded to g-C_3N_4.[40] The observed intimate interface was generally expected to be helpful for promote the separation of photogenerated carriers between C_3N_4 and $KNbO_3$ and thus improved the photocatalytic activity.

3.2. Photocatalytic activity of g-C_3N_4/$KNbO_3$ composite.

Fig. 6 displays the CH_4 evolution amounts over Pt loaded $KNbO_3$, g-C_3N_4, and g-C_3N_4/$KNbO_3$ composite photocatalysts. It was observed that the CH_4 was generated and increased with the prolongation of irradiation time over Pt loaded g-C_3N_4/$KNbO_3$ and g-C_3N_4 samples; while $KNbO_3$ showed hardly CH_4 generation under the same reaction conditions since $KNbO_3$ could be scarcely responsive to visible light. As shown in Fig. 6, the CH_4 generation amount over Pt-g-C_3N_4/$KNbO_3$ was higher than that of Pt-g-C_3N_4. Namely, during the first 8 h irradiation, the rate of CH_4 generation over Pt-g-C_3N_4/$KNbO_3$ was as high as 0.25 μmol h^{-1} in contrast to that of Pt-g-C_3N_4 (0.06 μmol h^{-1}), indicating that composite photocatalyst notably enhanced the photocatalytic performance compared with the naked photocatalyst. In order to check the repeatability of photocatalytic performance, the photocatalytic CO_2 reduction over used Pt-g-C_3N_4/$KNbO_3$ sample was performed again. It was worthwhile to note that the photocatalytic activity of used sample was similar to that of the fresh sample (See in Fig. S2). In order to investigate the structural stability, we checked XRD patterns of

pt-g-C_3N_4/$KNbO_3$ sample before and after the photocatalytic reaction. As shown in Fig. 7, there was no obvious peak variation was observed in the XRD patterns of pt-g-C_3N_4/$KNbO_3$ after the photocatalytic reaction, indicating that the phase of g-C_3N_4/$KNbO_3$ catalyst was relative stable without structural variation occurrence during the present photocatalytic reaction process.

3.3. Possible photocatalytic mechanism of g-C_3N_4/$KNbO_3$ composites.

One can see that, although g-C_3N_4/$KNbO_3$ and g-C_3N_4 have similar optical absorption, their photocatalytic activities in the photoreduction of CO_2 are apparently different. This implies that there should be another crucial factor that affects the photocatalytic activities notably. Actually, in addition to the optical absorption, the efficient charge separation of a semiconductor usually plays a crucial role in governing its photocatalytic performance. Herein, band potentials of g-C_3N_4 and $KNbO_3$ were investigated in order to clarify the charge separation in the g-C_3N_4/$KNbO_3$ interfaces. The band edge positions of photocatalysts were calculated using the following equation: $E_{VB} = X - E_e + 0.5E_g$, [68-71] where E_{VB} is the top of valance band (VB) relative to the normal hydrogen electrode (NHE); E_g means the band gap energy of the photocatalyst, E_e is the energy of free electrons (4.5 eV), X ($X=\sqrt[n]{X_1X_2X_3....X_n}$) is the geometric mean of the Mulliken electronegativity of the constituent atoms in the semiconductor. The Mulliken electronegativity of an atom is the arithmetic mean of the atomic electron affinity and the first ionization energy. Subsequently, VB edge potential of $KNbO_3$ was determined to be 2.39 eV relative to the normal hydrogen electrode (NHE), and E_{CB} of $KNbO_3$ was calculated to be -0.81 eV from the band gap in the view of the method inherent error (0.2 eV). While the CB and VB edge potentials of g-C_3N_4 were obtained to be -1.13 and 1.57 eV, respectively,

which was similar to the previous report.[62] It was noted that the VB top of $KNbO_3$ was lower than that of g-C_3N_4, while the CB bottom of C_3N_4 was higher than that of $KNbO_3$. In view of the above results and previous reports, [72-77] such a possible mechanism for the photocatalytic activity over the present g-C_3N_4/$KNbO_3$ is proposed and schematically illustrated in Fig. 8. The electron and hole pairs are excited upon light irradiation in g-C_3N_4, which serves as a sensitiser to absorb photons in the heterostructured photocatalysts. Subsequently, the photoexcited electrons on g-C_3N_4 could transfer to the CB of $KNbO_3$ since the CB edge potential of g-C_3N_4 (-1.13 eV) is more negative than that of $KNbO_3$ (-0.81 eV). It is generally acknowledged that noble metal Pt can act as a superior acceptor and trapping site for photo-excited electrons due to the different work function. Hence the photoinduced electrons would quickly transfer to the loaded Pt metal and then reduce CO_2 into CH_4. By such a vectorial electron transport manner, the photoexcited electron−holes in the heterostructured composite were spatially separated efficiently, resulting in an enhanced photocatalytic activity of g-C_3N_4/$KNbO_3$. In addition, the composition amount in the composite usually plays an important role in determining the photocatalytic activity. As shown in Fig. S3, all the g-C_3N_4/$KNbO_3$ composite samples exhibited higher CH_4 evolution amounts than pure g-C_3N_4. It was noted that the $KNbO_3$ content influenced the photocatalytic activities of the composites as-prepared materials notably. With an increase of $KNbO_3$ concentration from 15% to 25%, the photocatalytic activity increased and exhibited a CH_4 production yield of 1.94 μmol, which was more than four times higher than that of pure g-C_3N_4. However, excessive deposition of $KNbO_3$ possibly led to shielding the g-C_3N_4 surfaces, and subsequently decreased the photocatalytic activity.[51,55]

In order to verify the above-proposed mechanism, photoluminescence (PL) spectroscopy measurements were performed to analysis the process of charge carrier trapping and transfer. It is widely recognized that the lower fluorescence intensity means less recombination of photoinduced electron-hole pairs, leading to a higher photocatalytic activity. [78] As a reference, g-C_3N_4 and $KNbO_3$ with the same weight ratio as g-C_3N_4/$KNbO_3$ were also physically mixed. It was seen from Fig. S4 that pure g-C_3N_4 excited at 350 nm displayed a main emission peak at ~ 460 nm, which originated from the band–band PL process of self-trapped excitations.[79] The emission intensity of physically mixed g-C_3N_4-$KNbO_3$ was lower than that of pure g-C_3N_4 at a similar emission position, which could be primarily attributed to the decrease of g-C_3N_4 concentration.[51] As for g-C_3N_4/$KNbO_3$ composite, the emission intensity displayed an obvious decrease, suggesting that the recombination rate of carriers in the composite decreased due to photogenerated carrier transfer between g-C_3N_4 and $KNbO_3$, which was similar to the previous reports. [51,80] All these suggest some meaningful information to design an effective photocatalysts for CO_2 reduction.

4. Conclusion

In this study, a new kind of g-C_3N_4/$KNbO_3$ composite photocatalyst was successfully fabricated via introducing g-C_3N_4 on $KNbO_3$ and evaluated for CO_2 reduction under visible light irradiation. The HRTEM revealed that an intimate interface between C_3N_4 and $KNbO_3$ was formed in the composites. The resulting g-C_3N_4/$KNbO_3$ composite could absorb visible light region up to 460 nm. The photocatalytic activity of g-C_3N_4/$KNbO_3$ for CO_2 reduction was almost 4 times higher than that of individual g-C_3N_4 under visible light irradiation. Such a remarkable improvement of photocatalytic performance mainly originated from the improved

separation efficiency of photogenerated electron−hole pairs at the interface of g-C_3N_4/$KNbO_3$ composites, which could be ascribed to the well-aligned overlapping band-structures of C_3N_4 and $KNbO_3$. To sum up, the present research is expected to be a promising prospect for the development of composite photocatalysts for CO_2 conversion.

Acknowledgements

The authors would like to acknowledge the financial support from National Natural Science Foundation of China (Nos, 21203077, 51471077).

References

1. H. Q. Yang, Z. H. Xu, M. H. Fan, R. Gupta, R. B. Slimane, A. E. Bland and I. Wright, *J. Environ. Sci.*, 2008, **20**, 14–27.
2. M. Halmann, *Nature*, 1978, **275**, 115–116.
3. O. K. Varghese, M. Paulose, T. J. Latempa and C. A. Grimes, *Nano Lett.*, 2009, **9**, 731–737.
4. S. C. Roy, O. K. Varghese, M. Paulose and G. A. Grimes, *ACS Nano*, 2010, **4**, 1259–1278.
5. E. V. Kondratenko, G. Mul, J. Baltrusaitis, G. O. Larrazabalc and P. J. R. Amırez, *Energy Environ. Sci.*, 2013, **6**, 3112–3135.
6. Y. T. Liang, B. K. Vijayan, O. Lyandres, K. A. Gray and M. C. Hersam, *J. Phys. Chem. Lett.*, 2012, **3**, 1760−1765.
7. S. Navalón, A. Dhakshinamoorthy, M. lvaro and H. Garcia, *ChemSusChem*. 2013, **6**, 562–577.
8. H. F. Shi, T. Z. Wang, J. Chen, C. Zhu, J. H. Ye and Z. G. Zou, *Catal. Lett*., 2011, **141**, 525–530.
9. K. F. Li, X. Q. An, K. H. Park, M. Khraisheh and J. W. Tang, *Catal. Today*, 2014, **224**, 3–12.
10. T. Inoue, A. Fujishima, S. Konishi and K. Honda, *Nature*, 1979, **277**, 637–638.
11. W. N. Wang, W. J. An, R. Balavinayagam, S. Mukherjee, D. M. iedzwiedzki, S. Gangopadhyay and P. Biswas, *J. Am. Chem. Soc.*, 2012, **134**, 11276–11281.
12. L. J. Liu, H. L. Zhao, J. M. Andino and Y. Li, *ACS Catal*., 2012, **2**, 1817−1828.
13. V. Singh, J. C. B. Ignacio, C. R. Josep and N. Prashant, *Nano Lett.*, 2014, **14**, 597–603.
14. M. R. Hoffmann, J. A. Moss and M. M. Baum, *Dalton Trans.*, 2011, **40**,

5151–5158.

15. S. I. In, D. D. Vaughn and R. E. Schaak, *Angew. Chem. Int. Ed.*, 2012, **51**, 3915–3918.
16. A. Dhakshinamoorthy, S. Navalon, A. Corma and H. Garcia, *Energy Environ. Sci.*, 2012, **5**, 9217–9233.
17. A. Bazzo and A. Urakawa, *ChemSusChem*, 2013, **6**, 2095–2102.
18. K. Iizuka, T. Wato, Y. Miseki, K. Saito and A. Kudo, *J. Am. Chem. Soc.*, 2011, **133**, 20863–20868.
19. G. C. Xi, S. X. Ouyang, P. Li, J. H. Ye, Q. Ma, N. Su, H. Bai and C. Wang, *Angew. Chem. Int. Ed.*, 2012, **51**, 2395–2399.
20. N. H. Severin, S. M. Lukas and K. S. Jacek, *Angew. Chem. Int. Ed.*, 2013, **52**, 7372–7408.
21. M. Kazuhiko, D. L. Lu and K. Domen, *Angew. Chem. Int. Ed.*, 2013, **52**, 6488–6491.
22. Q. Liu, Y. Zhou, J. Kou, X. Chen, Z. Tian, J. Gao, S. Yan, and Z. G. Zou, *J. Am. Chem. Soc.*, 2010, **132**, 14385–14387.
23. N. Zhang, S. X. Ouyang, T. Kako and J. H. Ye, *Chem. Commun.*, 2012, **48**, 1269–1271.
24. K. Mori, H. Yamashita and M. Anpo, *RSC Adv.*, 2012, **2**, 3165–3172.
25. T. R. Gordon, M. Cargnello, T. Paik, F. Mangolini, R. T. Weber, P. Fornasiero and C. B. Murray, *J. Am. Chem. Soc.*, 2012, **134**, 6751−6761.
26. E. Balaraman, C. Gunanathan, J. Zhang, L. J. W. Shimon and D. Milstein, *Nat. Chem.*, 2011, **3**, 609−614.
27. C. A. Huff and M. S. Sanford, *J. Am. Chem. Soc.*, 2011, **133**, 18122−18125.
28. J. Liu, Y. Liu, N. Y. Liu, Y. Z. Han, X. Zhang, H. Huang, Y. Lifshitz, S. T. Lee, J.

Zhong and Z. H. Kang, *Science*, 2015, **347**, 970−974.

29. S. B. Yang, Y. J. Gong, J. S. Zhang, L. Zhan, L. L. Ma, Z. Y. Fang, R. Vajtai, C. X. Wang and M. A. Pulickel, *Adv. Mater.*, 2013, **25**, 2452–2456.
30. X. Maeda, Y. Wang, D. Nishihara, A. Lu, Antonietti and K. Domen, *J. Phys. Chem. C*, 2009, **113**, 4940–4947.
31. K. Wang, X. Maeda, K. Chen, K. Takanabe, Y. Domen, X. F. Hou and M. Antonietti, *J. Am. Chem. Soc.*, 2009, **131**, 1680–1681.
32. P. Niu, Y. Q Yang, J. C. Yu, G. Liu and H. M. Cheng, *Chem. Commun.*, 2014, **50**, 10837–10840.
33. S. C. Yan, Z. S. Li and Z. G. Zou, *Langmuir*, 2009, **25**, 10397–10401.
34. G. H. Dong and L. Z. Zhang, *J. Mater. Chem.*, 2012, **22**, 1160–1166.
35. J. Mao, T. Y. Peng, X. H. Zhang, K. Li, L. Q. Ye and L. Zan, *Catal. Sci. Technol.*, 2013, **3**, 1253–1260.
36. X. Wang, A. Maeda, K. Thomas, G. Takanabe, J. M. Xin, K. Carlsson, K. Domen and M. Antonietti, *Nat. Mater.*, 2009, **8**, 76–80.
37. H. F. Shi, C. L. Zhang and C. P. Zhou, *RSC Adv.*, 2015, **5**, 50146–50154.
38. L. M. Sun, X. Zhao, C. J. Jia, Y. X. Zhou, X. F. Cheng, P. Li, L. Liu and W. L. Fan, *J. Mater. Chem.*, 2012, **22**, 23428–23438.
39. Y. J. Wang, R. Shi, J. Lin and Y. F. Zhu, *Energy Environ. Sci.*, 2011, **4**, 2922–2929.
40. C. S. Pan, J. Xu, Y. J. Wang, D. Li and Y. F. Zhu, *Adv. Funct. Mater.*, 2012, **22**, 1518−1524.
41. N. Yang, G. Q. Li, W. L. Wang, X. L. Yang and W. F. Zhang, *J. Phys. Chem. Solids.*, 2011, **72**, 1319–1324.
42. G. Q. Li, N. Yang, W. L. Wang and W. F. Yang, *J. Phys. Chem. C*, 2009, **113**,

14829–14833.

43. J. Y. Zhang, Y. H. Wang, J. Jin, J. Zhang, Z. Lin and F. Huang, J. G. Yu, *ACS Appl. Mater. Interfaces*, 2013, **5**, 10317–10324.
44. C. S. Pan, J. Xu, Y. J. Wang, D. Li and Y. F. Zhu, *Adv. Funct. Mater.*, 2012, **22**, 1518–1524.
45. L. M. Sun, X. Zhao, C. J. Jia, Y. X. Zhou, X. F. Cheng, P. Li, L. Liu and W. L. Fan, *J. Mater. Chem.*, 2012, **22**, 23428–23438.
46. F. Chang, Y. Xie, J. Zhang, J. Chen, C. Li, J. Wang, J. Luo, B. Deng and X. Hu, RSC Adv., 2014, **4**, 28519–28528.
47. J. Chen, S. Shen, P. Guo, P. Wu and L.J. Guo, *J. Mater. Chem. A*, 2014, **2**, 4605–4612.
48. G. G. Zhang, S. H. Zang and X.C.Wang, *ACS Catal.* 2015, **5**, 941−947.
49. W. Zhao, Y. Guo, S. Wang, H. He, C. Sun and S. G. Yang, *Appl. Catal., B*, 2015, **165**, 335–343.
50. Z.W. Zhao, Y.J. Sun, and F. Dong, *Nanoscale*, 2015, **7**, 15-37.
51. Y. M. He, L. H. Zhang, B. T. Teng and M. H. Fan, *Environ. Sci. Technol.*, 2015, **49**, 649−656.
52. S. Zhou, Y. Liu, J. M. Li, Y. J. Wang, G. Y. Jiang, Z. Zhao, D. Wang, A. J. Duan, J. Liu and Y. C. Wei, *Appl. Catal. B: Environ.*, 2014, **158**, 20–29.
53. M. L. Li, L. X. Zhang, X. Q. Fan, Y. J. Zhou, M. Y. Wu and J. L. Shi, *J. Mater. Chem. A*, 2015, **3**, 5189–5196.
54. Y. P. Yuan, S. W. Cao, Y. S. Liao, L. S. Yin and C. Xue, *Appl. Catal. B. Environ.*, 2013, **140**, 164–168.
55. S. W. Cao, X. F. Liu, Y. P. Yuan, Z. Y. Zhang, Y. S. Liao, J. Fang, C. J. L. Say, T. C. Sum and C. Xue, *Appl. Catal. B: Environ.*, 2014. **147**, 940–946.

56. H. F. Shi and Z. G. Zou, *J. Phys. Chem. Solids*, 2012, **73**, 788–792.

57. L. Q. Jiang, Y. Qiu and Z. G. Yi, *J. Mater. Chem. A*, 2013, **1**, 2878–2885.

58. Q. Ding, Y. Yuan, X. Xiong, R. Li, H. Huang, Z. Li, T. Yu, Z. G. Zou and S. Yang, *J. Phys. Chem. C*, 2008, **112**, 18846-18848.

59. T. T. Zhang, K. Zhao, J. G. Yu, J. Jin, Y. Qi, H. Q. Li, X. J. Hou and G. Liu, *Nanoscale*, 2013, **5**, 8375-8383.

60. L. S. Yan, J. Zhang, X. M. Zhou, X. X. Wu, J. Y. Lan, Y. S. Wang, G. Liu, J. G. Yu and L. J. Zhi, *Int. J. Hydrogen Energy*, 2013, **38**, 3554–3561.

61. J. Yu, K. Wang, W. Xiao and B. Cheng, *Phys. Chem. Chem. Phys.*, 2014, **16**, 11492–11501.

62. H. F. Shi, G. Q. Chen, C. L. Zhang and Z. G. Zou, *ACS Catal.*, 2014, **4**, 3637–3643.

63. H. Q. Pan, X. K. Li, Z. J. Zhuang and C. Zhang, *J. Mol. Catal. A: Chem.*, 2011, **345**, 90–95.

64. Y. Wang, X. Wang and M. Antonietti, *Angew. Chem. Int. Ed.*, 2012, **51**, 68–89.

65. A. Vinu, *Adv. Funct. Mater*., 2008, **18**, 816–827.

66. Q. J. Xiang, J. G. Yu, and M. Jaroniec, *J. Phys. Chem. C*, 2011, **115**, 7355–7363.

67. J. X. Sun, Y. P. Yuan, L. G. Qiu, X. Jiang, A. J. Xie, Y. H. Shen and J. F. Zhu, *Dalton Trans.*, 2012, **41**, 6756−6763.

68. A. H. Nethercot, *Phys. ReV. Lett.*, 1974, **33**, 1088.

69. M. A. Butler and D. S. Ginley, *J. Electrochem. Soc.*, 1978, **125**, 228-232.

70. H. F. Shi, Z. Li, J. Kou, E. J. Ye and Z. G. Zou, *J. Phys. Chem. C*, 2011, **115**, 145−151.

71. H. F. Shi, G. Q. Chen and Z. G. Zou, *Appl. Catal. B. Environ.*, 2014, **156**–**157**, 378–384.

72. X. C. Wang, S. Blechert and M. Antonietti, *ACS Catal*., 2012, **2**, 1596−1606.

73. R. Marschall, *Adv. Funct. Mater.*, 2014, **24**, 2421–2440.

74. H. Xu, J. Yan, Y. Xu, Y. Song, H. Li, J. Xia, C. Huang and H. Wan, *Appl. Catal. B. Environ*., 2013, **129**, 182–193.

75. A. Kumar, T. Surendar, A. Baruah and V. Shanker, *J. Mater. Chem. A*, 2013, **1**, 5333–5340.

76. S. Cao and J. Yu, *J. Phys. Chem. Lett*., 2014, **5**, 2101−2107.

77. X. J. Guan and L. J. Guo, *ACS Catal*., 2014, **4**, 3020–3026.

78. M. R. Hoffmann, S. T. Martin, W. Y. Choi and D. W. Bahnemann, *Chem. ReV.*, 1995, **95**, 69−96.

79. X. H. Zhang, L. J. Yu, C. S. Zhuang, T. Y. Peng, R. J. Li and X. Li, *J. ACS Catal*., 2014, **4**, 162−170.

80. X. J. Wang , X. Tian , F. Li , Jun Zhao , Y.p. Li , R. H. Liu and Y.J. Hao, *Dalton Trans*., 2015, **44**, 17859–17866.

Figure captions

Fig. 1 XRD patterns of pure g-C_3N_4, $KNbO_3$, and g-C_3N_4/$KNbO_3$ composite photocatalysts.

Fig. 2 UV-vis diffuse reflectance spectra for pure g-C_3N_4, $KNbO_3$, and g-C_3N_4/$KNbO_3$ composite photocatalysts.

Fig. 3 XPS spectra of the samples: (a) C 1s peaks of g-C_3N_4/$KNbO_3$ and g-C_3N_4; (b) N 1s peaks of g-C_3N_4/$KNbO_3$ and g-C_3N_4; (c) K 2p peaks of $KNbO_3$ and g-C_3N_4/$KNbO_3$; (d) Nb 3d peaks of $KNbO_3$ and g-C_3N_4/$KNbO_3$; (e) O 1s peaks of $KNbO_3$ and g-C_3N_4/$KNbO_3$.

Fig. 4 FE-SEM images of (a) g-C_3N_4, (b) $KNbO_3$, and (c) g-C_3N_4/$KNbO_3$.

Fig. 5 (a) TEM and (b) HRTEM images of g-C_3N_4/$KNbO_3$ heterojunction.

Fig. 6 CH_4 evolution amounts over Pt loaded g-C_3N_4, $KNbO_3$, and g-C_3N_4/$KNbO_3$ composite photocatalysts.

Fig. 7 XRD patterns for Pt-g-C_3N_4/$KNbO_3$ composite photocatalyst before and after photocatalytic reaction.

Fig. 8 Schematic illustrations of photocatalytic reaction over Pt-g-C_3N_4/$KNbO_3$ composite under visible light irradiation.

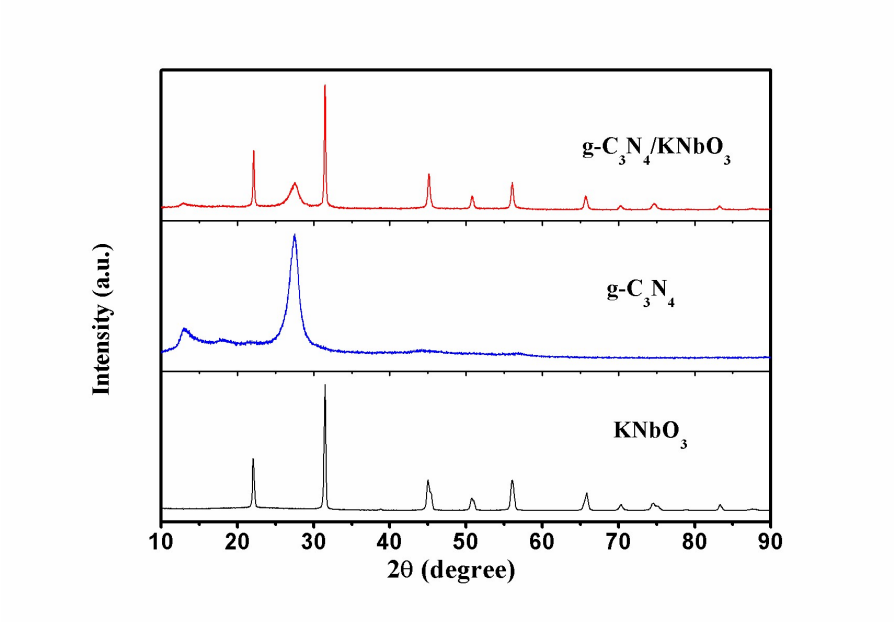

Fig. 1

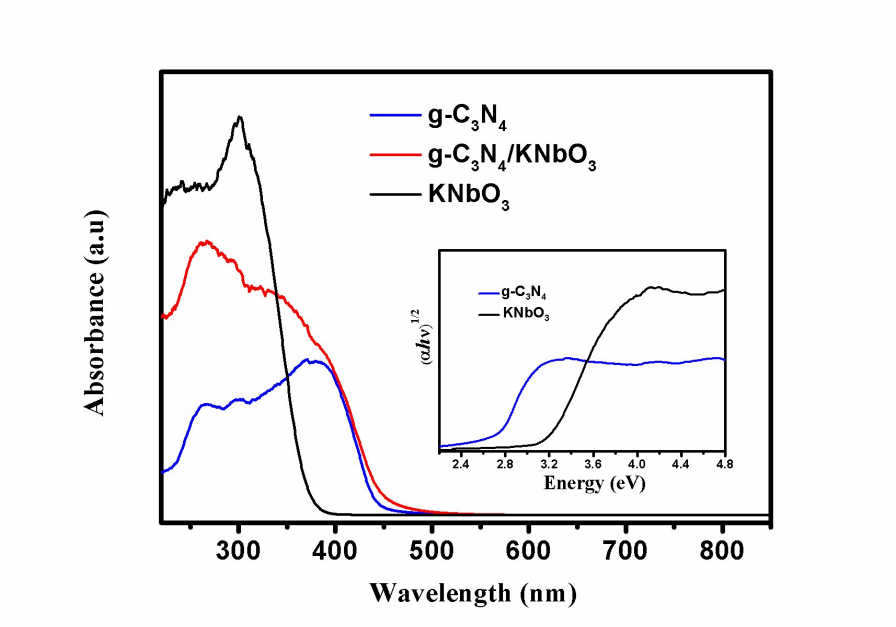

Fig. 2

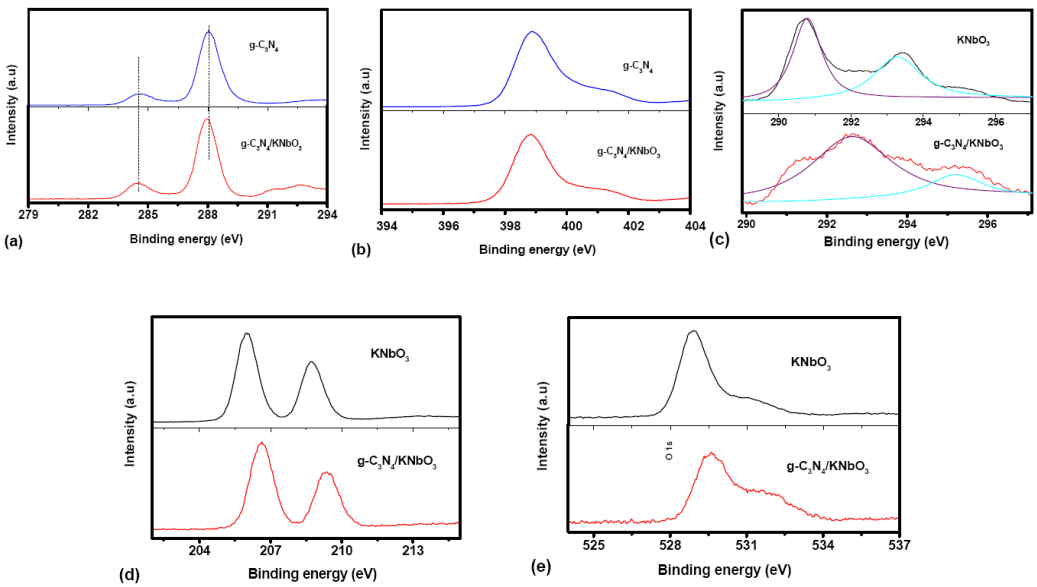

Fig. 3

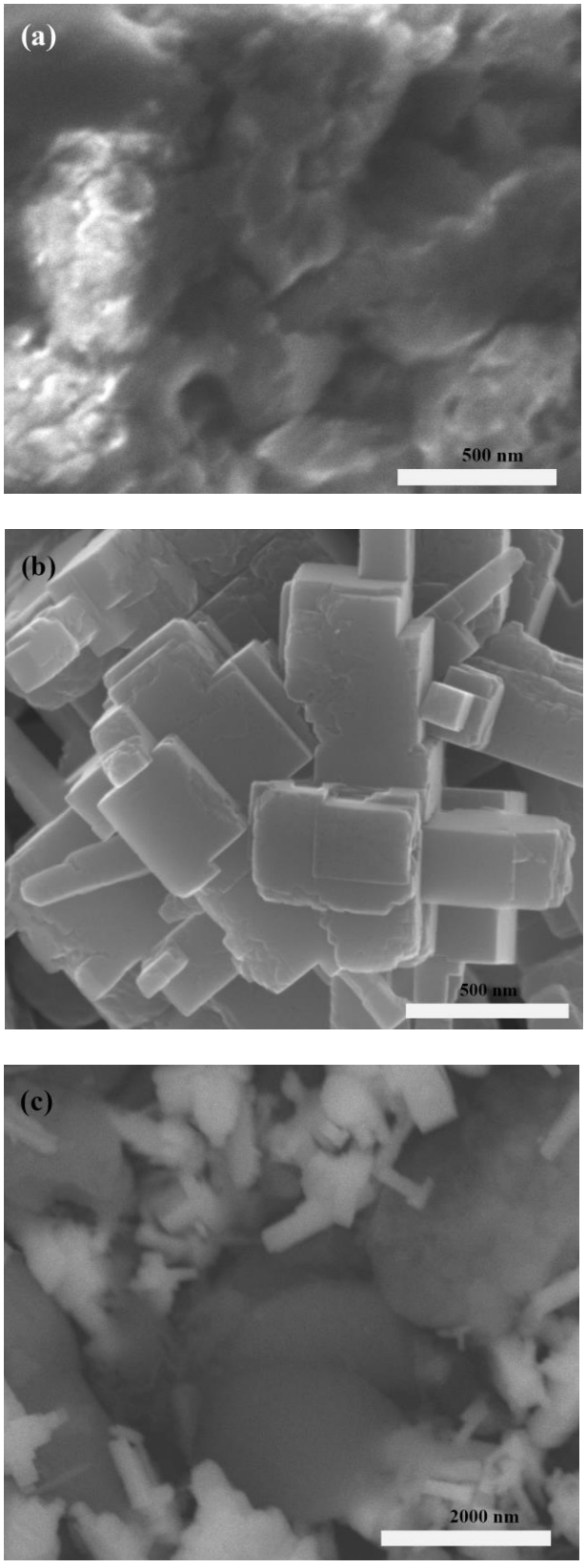

Fig. 4

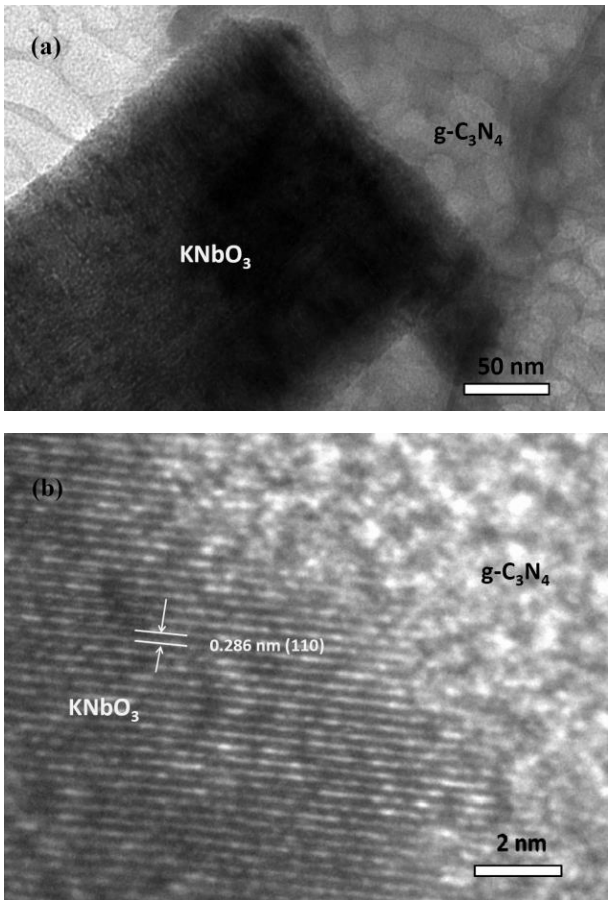

Fig. 5

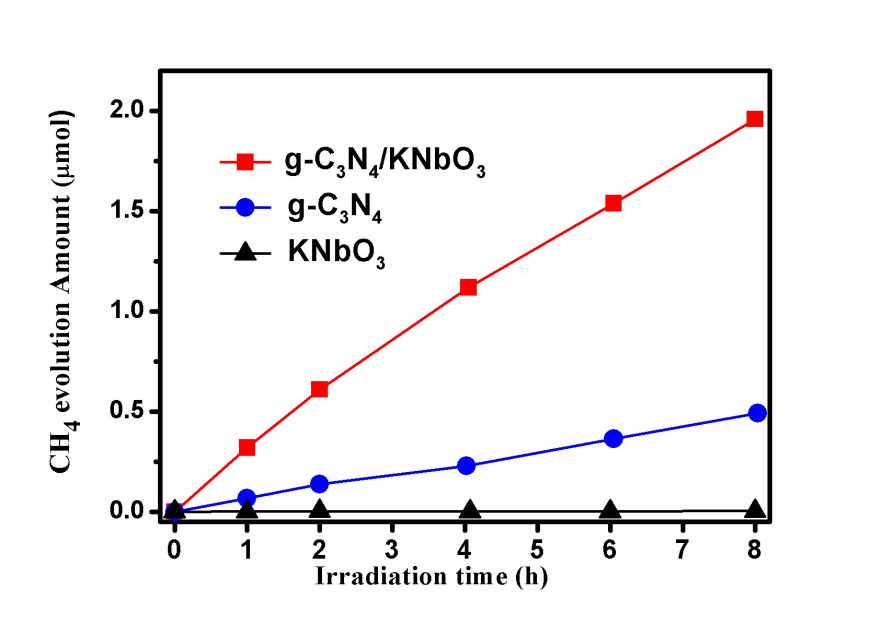

Fig. 6

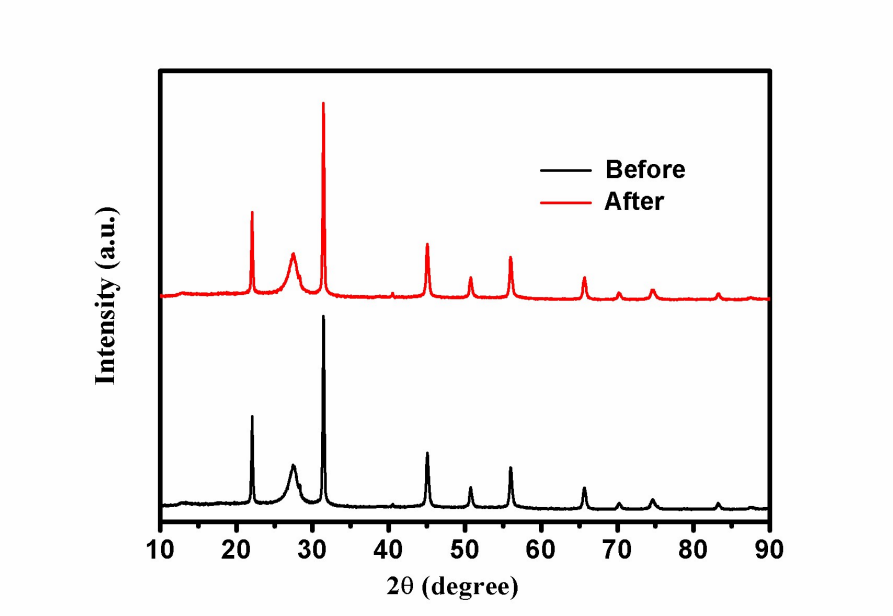

Fig. 7

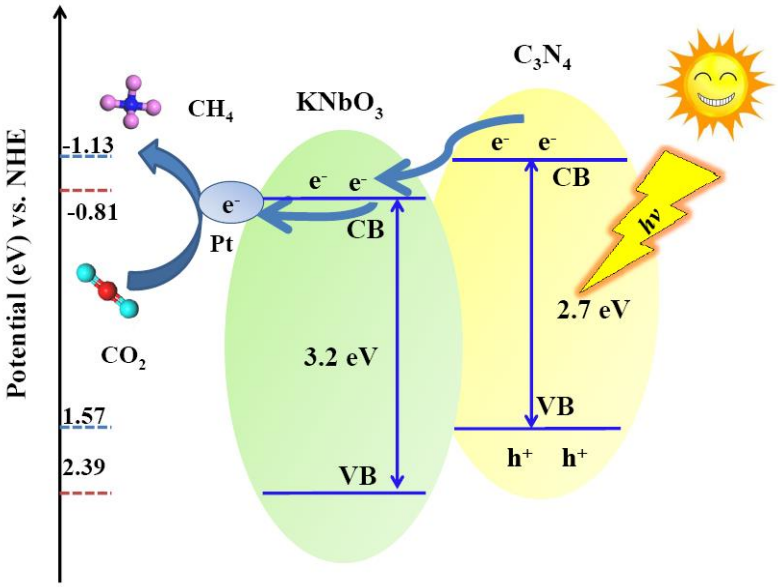

Fig. 8